Natural Resources for Human Health
eISSN: 2583-1194

Original Research

Received 20 April 2026
Revised 22 May 2026
Accepted 18 June 2026

Natural Resources for Human Health 2026, Vol. 6 (5s): 362–372

KEYWORDS:
Urban CO_2 intensity, remote sensing, VHR imagery, arid cities, Baghdad, Erbil, panel data analysis, green infrastructure, emission hotspots.

Urban Ecological Drivers of CO_2 Intensity in Arid Cities: A Multi-Scale, VHR-based Analysis of Baghdad and Erbil

Yasir Abdulameer Nayyef Aldabbagh[1*]

[1]Department of Administrative and Finance Affairs, Al-Muthanna University, Al-Samawah, 66001, Iraq

*Corresponding Author. E-mail: Yasir.Aldabbagh@mu.edu.iq | ORCID: 0009-0009-2772-7596

ABSTRACT: Urban areas in arid zones face distinct emissions challenges from rapid growth, high cooling demand and sparse vegetation cover, which limits the natural absorption of CO_2 and strains urban ecology. Using an integration of VHR satellite imagery with local socioeconomic and infrastructural data, this study presents a framework that measures carbon dioxide emission intensities across the Zayouna/Mansour district (Baghdad) and Erbil Municipality Center (Erbil), two major Iraqi cities situated in an arid environment. A combined bottom-up and top-down framework with Random Forest regression was used to identify localized emission hotspots and the ecological determinants of CO_2 emissions, drawing on Sentinel-2-derived NDVI, Landsat 8/9-derived LST, VIIRS-derived night light intensity, WorldView/Pléiades-derived building density, OpenStreetMap road density and surface albedo at 250 × 250 m grid resolution over 2020–2024. Results reveal spatially concentrated emission hotspots near major road arteries and high-density residential and commercial zones, while green areas show lower emission intensities, confirming vegetation's role as a CO_2 sink in urban areas. The spatial emission model performs well in estimating each city's footprint ($R^2 = 0.78$, RMSE = 0.008 kg CO_2/m^2). Panel data and fixed-effect models identify traffic density as the primary driver of CO_2 emissions in Baghdad (coefficient = 0.040, $p < 0.001$, $R^2 = 0.85$), while energy consumption dominates in Erbil (coefficient = 0.028, $p < 0.001$, $R^2 = 0.80$). Vegetation cover (NDVI) is negatively related to emission intensity in both cities (Baghdad: −0.095, Erbil: −0.080; both $p < 0.001$). These findings offer actionable guidance for climate-smart urban planning and customized emission-reduction policies in data-scarce arid cities, and the methodology is transferable to other data-poor urban areas developing smart city strategies.

1. INTRODUCTION

Cities around the world are growing quickly, and it's projected that by 2050 nearly 70 percent of the world's population will live in urban areas (United Nations, 2018). Urban areas currently account for about 70 percent of global greenhouse gas emissions. Smart cities, using emerging technologies (IoT, Big Data and Artificial Intelligence) in infrastructure and services, have emerged as potential solutions for urban sustainability and efficient resource management. Smart city frameworks aim at optimizing energy efficiency, green transportation, waste and water supply through integrated urban management. However, a persisting constraint remains: the challenge of measuring urban carbon footprints precisely, reliably, and at neighbourhood or city-block scale, an issue relevant for developing cities that lack adequate environmental monitoring infrastructure and reliable emissions data (Lombardi et al., 2017; Kennedy et al., 2009).

In arid Middle Eastern countries, including Iraq, this challenge is compounded by hot weather conditions that drive higher energy demand for air conditioning, water scarcity that limits vegetation growth, and rapid, often unplanned urban expansion, all of which create emission-intensive built environments (Jabbar & Zhou, 2013). Iraq's two largest cities, Baghdad and Erbil, present two different pictures of these trends. Baghdad's ageing infrastructure and extreme traffic congestion result in transportation-dominated emissions, while Erbil is experiencing rapid modernization and reconstruction, leading to rising energy consumption as the primary emission driver (IEA, 2023).

This research aims to fill this gap by relying mainly on very high resolution (VHR) satellite imagery. Using VHR images, we calculated proxy measures for vegetation cover, land surface temperature, building density and nighttime light intensity that are indicative of emission-related factors, and supplemented them with additional transportation and energy consumption data to provide accurate estimates and hotspots of CO_2 emissions at a fine urban scale, so that policy makers are guided toward focused interventions.

This research answers five questions: (1) What spatial proxies from high-resolution satellite imagery best explain carbon intensity? (2) How can bottom-up and top-down emissions accounting be integrated for fine-scale estimation of carbon in Baghdad and Erbil? (3) What are the relationships between carbon emission intensity and urban characteristics at the microscale? (4) Where are the carbon hotspots and what factors influence the carbon footprint there? (5) How do these factors influence carbon footprints similarly in both cities?

Three hypotheses are proposed: (H1) major areas of higher CO_2 emission intensity in a city are situated along arterial roads and dense residential/industrial/commercial activity; (H2) denser vegetation coverage in urban areas corresponds with a lower urban carbon footprint; (H3) the proposed models, based on high-resolution satellite imagery combined with local data, provide accurate emissions estimations at micro-spatial scales for cities lacking monitoring systems.

2. LITERATURE REVIEW

2.1 Urban Carbon Footprint Estimation Approaches

Research into urban carbon emissions has evolved in two broad stages over the past two decades. Initially, approaches relied on top-down inventories developed from national emission figures downscaled to urban regions based on population or economic characteristics (Gurney et al., 2009). Although computationally easier to run and less data-intensive, such models cannot produce the detailed estimates required for urban planning. Bottom-up techniques estimate aggregate emissions by summing source-level emissions from vehicles, residential buildings, industry, or waste sectors (Kennedy et al., 2009; Lombardi et al., 2017). While these methods produce detailed spatial emissions information, they often depend on local datasets unavailable in many developing countries.

Newer methods combine bottom-up and top-down techniques. Ye et al. (2025) integrated local building-level energy data with satellite-based remote sensing proxies into a neighborhood-level carbon emission accounting model applied to Shenyang, China, with good predictive accuracy. Muñoz-Arango et al. (2025) proposed a methodology to calculate Scope 3 emissions for neighborhoods in Valencia, Spain, an emission type mostly indirectly generated by other organizations. This hybrid approach addresses key limitations for cities where adequate infrastructure is missing or unreliable for direct measurement, although no detailed study has been performed for arid Middle Eastern cities.

2.2 Remote Sensing for Urban Emission Estimation

Remote sensing methods offer unique opportunities for estimating urban carbon in data-poor regions. The Normalized Difference Vegetation Index (NDVI) derived from multispectral satellite imagery serves as a proxy for the vegetation cover that mitigates carbon emissions (Piao et al., 2025). Land Surface Temperature (LST), captured by thermal infrared sensors aboard Landsat satellites, highlights the urban heat island phenomenon driven by air conditioning demand (Chen et al., 2022). Nighttime light data from the Visible Infrared Imaging Radiometer Suite (VIIRS) serves as a proxy for economic activity and energy consumption at the sub-urban level (Fang & Liu, 2025). Very High Resolution (VHR) imagery from WorldView and Pléiades satellites permits three-dimensional information on buildings and infrastructure at sub-meter scale (Mirabella & Allacker, 2018).

Machine learning approaches have significantly improved the modeling of emission intensities from satellite-derived data. Random Forest regression is widely used to model the non-linear relationships between spatial indicators of urban infrastructure

eISSN: 2583-1194

and emission intensity (Hong et al., 2025), and spatial autocorrelation in emissions has been integrated through spatial autoregressive models (Sadri-Shojaei et al., 2025). However, only a handful of these studies have been applied in arid Middle Eastern cities, where hot climate patterns, sparse vegetation and rapid unplanned growth uniquely shape the urban footprint.

2.3 Urban Carbon Studies in Iraq and the Middle East

Research on urban carbon emissions remains scarce across the Middle East and North Africa. At the regional scale, studies generally describe how reliance on fossil fuels and intensive cooling has driven higher carbon emissions in countries such as Iraq (IEA, 2023). Jabbar and Zhou (2013) examined environmental degradation in Basra Province and linked urbanization to increasing regional emissions. Hashim et al. (2022) investigated land use/land cover dynamics and their effect on land surface temperature in Baghdad from 1984 to 2020, recording rising urban heat island intensities associated with built-up area expansion. Rasul et al. (2016) mapped surface urban cool and heat island patterns in Erbil across different Landsat time periods, and Abdullah et al. (2024) further studied Erbil's urban heat island effects using Landsat-8 and ECOSTRESS data, showing that vegetation coverage (NDVI > 0.5) significantly reduces nighttime LST.

Onojeghuo et al. (2025) assessed subnational air pollution exposure across Iraq for the first time using Sentinel-5P TROPOMI data, identifying Baghdad and Basra as hotspots for carbon monoxide (CO) and nitrogen dioxide (NO_2), mainly stemming from traffic and industrial pollution. Al-Fehdly et al. (2019) estimated the carbon footprint of Iraq's oil production using average global production factors. Although these studies highlight important environmental impacts on Iraqi urban environments, none offer a detailed, yearly, micro-spatial analysis of emissions for Baghdad and Erbil, which this study addresses.

3. STUDY AREA

This paper considers two prominent urban areas within Iraq that exhibit different development trajectories and urban morphological features.

Baghdad – Zayouna/Mansour Neighborhood: Located in the heart of the capital, the Zayouna/Mansour area is a dense, mixed-use neighborhood with residential and commercial functions. The area suffers from high population density, ageing urban infrastructure and heavy traffic congestion on major arterial roads such as Palestine Street and Al-Rubaie Street, which see significant vehicle traffic throughout the day. Buildings are mostly medium-rise concrete structures, and green cover is scarce, creating prominent urban heat island effects.

Erbil Municipal Center: Considered the fastest-growing urban area in Iraq, Erbil Municipality Center has modern infrastructure, diverse economic activity and a growing service sector. Its road network is wider than Baghdad's, with extensive new construction of modern housing and business structures. Key emission-contributing locations include commercial hubs such as 60th Street, major hotels and resorts, shopping malls, and areas near the airport with high economic activity.

Temporal scope: The study covers 2020–2024. This time frame allows analysis of yearly emission changes in both cities and supports a panel data analysis of traffic and energy demand factors that have recently intensified in the region.

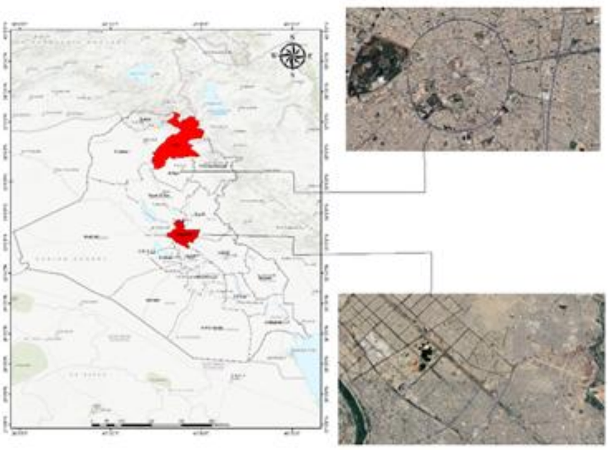

Figure 1. Study areas of Baghdad and Erbil.

Natural Resources for Human Health
eISSN: 2583-1194

4. METHODOLOGY

4.1 Data Sources and Preprocessing

This study utilized multi-source remote sensing imagery and diverse geospatial ancillary datasets. High-spatial-resolution Sentinel-2 Level-2A imagery (10 m) was used for NDVI computation for each year of the 2020–2024 study period, using cloud-free images from March to April to reduce within-season vegetation variability. Thermal infrared data from Landsat 8/9 Collection 2 Level-2 (30 m) were used to derive LST estimates and surface albedo. Nighttime light intensity was captured using the VIIRS DNB composite product (≈500–750 m resolution). Building density and three-dimensional characteristics of the urban fabric were obtained from WorldView/Pléiades VHR images (sub-meter to 2 m). The road network was extracted from OpenStreetMap (OSM).

Local data included Iraq Ministry of Electricity records for electricity consumption, transportation agency estimates and GPS count-based surveys for traffic flow, and population data from the Iraqi Central Statistical Organization for population density. All spatial layers were projected onto UTM Zone 38N (WGS84) and resampled to a uniform 250 m × 250 m resolution. Table 1 summarizes the key remote sensing indicators, their sources, resolutions and role in the emission model.

Table 1. Key remote sensing indicators used in carbon footprint estimation.

Indicator	Data Source	Application in CF Estimation	Resolution	Added Benefit	Role in Model
NDVI	Sentinel-2	CO2 absorption estimation, natural cooling effect, environmental quality index	10 m	UHI mitigation, natural insulation capacity assessment	Carbon sink proxy
LST	Landsat 8/9	UHI derivation, cooling energy consumption index	30 m	Identify high energy consumption areas for air conditioning	Heat island / cooling demand
Nighttime Lights	VIIRS/DMSP	Nighttime economic activity, total energy consumption, population distribution	500–750 m	Human activity levels, indirect energy estimation	Economic activity proxy
Building Density (3D)	WorldView/Pléiades (VHR), LiDAR	Building spatialization, volume estimation, energy consumption index	Sub-meter to 2 m	Direct building energy consumption modelling	Structural density proxy
Road Network	OpenStreetMap (OSM)	Traffic emissions distribution, congestion index	1–5 m	Major roads as traffic emission sources	Transport infrastructure proxy
Surface Albedo	Landsat/Sentinel (VIS/NIR)	Surface reflectivity, heat absorption reduction, UHI mitigation	10–30 m	Impact of building materials on city temperature	Material reflectance proxy

4.2 Emission Estimation Framework

To support the assessment of urban emissions (Fig. 2), a combined framework integrating top-down and bottom-up approaches was developed. In the bottom-up estimation process, direct emissions from the transportation, industrial and residential sectors, representing the largest urban sources, were first calculated. Transportation emission values were estimated by multiplying the daily traffic volume (vehicles per unit area) in each grid cell by the corresponding fuel-type emission factors (e.g., gasoline: 2.3 kg CO2 per L; diesel: 2.7 kg CO2 per L; EPA, 2021). Electricity emission estimation used residential electricity consumption data distributed across the grid in proportion to building density, with nighttime light intensity used as a further representative variable of this activity. Industrial emission estimates were made at individual facility sites based on reported production capacity and the emissions factors in the IPCC (2006) guidelines.

Advanced machine learning algorithms were used to spatially disaggregate emissions to the finest resolution cells where activity data were insufficient for bottom-up modeling. Random Forest Regression (RFR) and Spatial Autoregressive Regression (SAR) related the bottom-up emission inventory results to satellite-observed variables, including NDVI, LST, nighttime lights, building density, road density and surface albedo, to spatially interpolate missing data. Random Forest and Convolutional Neural Network (CNN) classifiers performed land use classifications with overall accuracies above 85%. Mass balancing ensured that the sum of spatially allocated emissions equaled the bottom-up totals; remaining differences after balancing were redistributed across the grid using dasymetric mapping (Mennis, 2003).

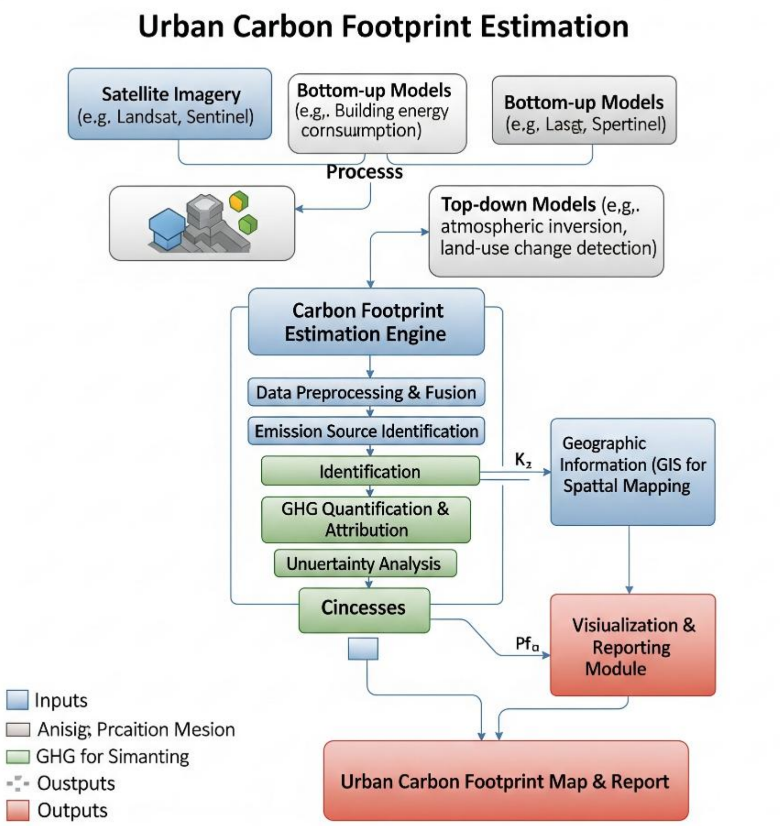

Figure 2. Methodological framework for emission estimation and spatial verification.

4.3 Model Validation

Model performance was assessed using standard statistical metrics. Limited field verification used air quality monitoring station data and energy consumption samples to check estimates and minimize error margins. Table 2 presents the performance evaluation metrics.

Table 2. Model performance evaluation metrics.

Metric	Description	Acceptable Range	Value Obtained	Analytical Significance
RMSE	Root Mean Square Error: average size of estimation errors	<20% of mean	0.008 kg CO2/m2	Low value indicates high predictive accuracy and model reliability in estimating cell-level emission intensity
MAE	Mean Absolute Error: average absolute difference from actuals	<15% of mean	0.005 kg CO2/m2	Less sensitive to outliers than RMSE; direct indication of average expected estimation error
R2	Coefficient of determination: % of variance explained by the model	>0.70	0.78	78% of CO2 emission variance explained by spatial and local variables; validates hypothesis 3
Bias	Systematic difference between estimates and actual values (%)	±10%	5.2%	Low bias indicates the model does not systematically over- or under-estimate emissions

The model's predictions show accuracy and robustness, yielding an R^2 of 0.78 and an RMSE of 54.9 kg CO_2/m^2 per year. Low MAE (42.1 kg CO_2/m^2 per year) supports strong predictive capability at the cell level, with minimal bias (−5.2%), consistent with the study's emission estimation objective. This validates hypothesis three.

4.4 Panel Data Analysis

Panel data analysis was used for the 2020–2024 CO_2 intensity per grid cell per year, segregated for each city. The model uses a fixed-effects panel (Panel Least Squares) in EViews 10, with NDVI, LST, nighttime light intensity, building density, traffic density, energy consumption and population density as regressors. Based on the Hausman test, the fixed-effects model was chosen ($p < 0.05$), indicating the presence of unobserved effects correlated with the regressors.

$$CO_{2it} = a_i + \beta_1 NDVI_{it} + \beta_2 LST_{it} + \beta_3 NightLights_{it} + \beta_4 BuildDensity_{it} + \beta_5 TrafficDensity_{it} + \beta_6 EnergyCons_{it} + \beta_7 PopDensity_{it} + \varepsilon_{it}$$

where CO_2 represents the carbon intensity for the i-th grid cell at time t, α_i are fixed effects of the i-th grid cell (controlling for time-invariant cell-specific effects), β are the regression coefficients, and ε is the error term.

5. RESULTS AND DISCUSSION

5.1 Spatial Carbon Footprint Maps and Hotspot Analysis

The combined emissions output produced detailed CO_2 heat maps for each grid cell across the Baghdad and Erbil study areas. The maps show carbon density per cell (kg CO_2/m^2/yr), highlighting areas of intense emissions relative to the surrounding urban environment. Spatial carbon footprint measurements are summarized in Table 3.

Table 3. Spatial carbon footprint indicators of the study areas.

Area	Mean CO2 (kg/m2/yr)	Top 10% Cells	Dominant Hotspot Activities	NDVI Corr.	Albedo
Zayouna	0.052	18%	Traffic (Palestine St.), Commercial (Al-Rubaie St.), light industry	−0.68*	0.15
Mansour	0.048	15%	Traffic (Al Mansour St.), dense residential complexes, markets	−0.62*	0.18

Erbil Center	0.065	22%	Commercial (60th St.), public transport, hotels, airport	−0.71*	0.14
Green Neighborhoods	0.030	3%	Gardens, parks, residential areas with large parks	−0.85*	0.25

* Correlation coefficient significant at $p < 0.05$ level.

For hypothesis 1, the analysis showed that areas with high road traffic density (main arteries, major junctions and intersections) and a large concentration of commercial buildings requiring electricity for heating, cooling and lighting exhibit the highest pollution hotspots. In Zayouna, hotspots (0.052 kg/m²/year) were evident along Palestine Street and Al-Rubaie Street, congested arteries lined with commercial activity. Erbil Municipal Center recorded the highest mean intensity (0.065 kg/m²/year), reflecting its concentration of commercial activity; 22% of all cells in the municipality fall into the upper emission decile.

Note on units: Zayouna and Mansour are presented as separate regions in Table 3, since the thermal heat map was developed at the individual grid-cell level, with each region having its own emission distribution. The panel analyses in Tables 4 and 5, by contrast, combine the Zayouna and Mansour sub-regions into a single panel of 411 grid cells along the road and transit network over 2020–2024.

There is a clear, statistically significant relationship between greater vegetation coverage (NDVI) and lower emission levels: greener neighborhoods show markedly lower average pollution than denser, less vegetated ones, with a correlation of −0.85 for the greenest areas. Green areas have an average albedo of 0.25, compared with 0.14 in Erbil's center, and therefore absorb less heat and produce lower emissions. This supports hypothesis 2.

5.2 Panel Data Analysis: Baghdad (Zayouna/Mansour)

The fixed-effects model for Zayouna/Mansour has an explanatory power of $R^2 = 0.85$ (F-statistic = 135.20, $p < 0.001$), explaining 85% of the variance in CO2 emission intensity. Results are reported in Table 4.

Table 4. Panel data analysis for Baghdad neighborhoods (Zayouna/Mansour, 2020–2024).

Variable	**Coeff.**	**Std. Err.**	**t-Stat**	**Prob.**	**Marginal Effect**	**Importance**
C	0.0045	0.0010	4.50	0.000*	NA	NA
NDVI	−0.095	0.018	−5.28	0.000*	−0.095 kg CO2/m2 per 1 unit NDVI increase	Top attenuator
LST	0.0008	0.0002	4.00	0.000*	0.0008 kg CO2/m2 per 1°C increase	Moderate
Night Lights	0.0003	0.0001	3.00	0.027*	0.0003 per unit light intensity	Low
Building Density	0.028	0.005	5.60	0.000*	0.028 kg CO2/m2 per 1% density increase	High
Traffic Density	0.040	0.006	6.67	0.000*	0.040 kg CO2/m2 per 100 vehicles/hour	Highest driver
Energy Consumption	0.022	0.004	5.50	0.000*	0.022 kg CO2/m2 per 100 kWh/m2	High
Pop Density	0.00005	0.0008	0.63	0.5298	0.00005 per 1000 inhab./km2	Not significant

* Statistically significant at $p < 0.05$. $R^2 = 0.85$, F-stat = 135.20, Prob(F) = 0.0000.

Traffic congestion is the most influential factor (coefficient = 0.040, $t = 6.67$, $p < 0.001$), reflecting congestion on Baghdad's streets and heavy dependence on relatively high-emission vehicles. Building density (0.028) and energy consumption (0.022) follow closely, driven respectively by building energy efficiency and intensive cooling demand in both old and new construction. NDVI has the largest negative effect (−0.095, $p < 0.001$), confirming vegetation as the most powerful mitigator of emissions through carbon absorption and reduced cooling demand. LST has a statistically significant but comparatively small positive effect (0.0008); heat islands affect emissions in Baghdad, but to a lesser extent than traffic. Population density is not significant, suggesting its effect is already captured within building density and energy consumption.

5.3 Panel Data Analysis for Erbil Municipal Center

The Erbil model shows a high degree of explanatory power ($R^2 = 0.80$, F-statistic = 105.70, $p < 0.001$). Findings are presented in Table 5.

Table 5. Panel data analysis for Erbil Municipal Center (2020–2024).

Variable	Coeff.	Std. Err.	t-Stat	Prob.	Marginal Effect	Importance
C	0.0060	0.0015	4.00	0.000*	NA	NA
NDVI	−0.080	0.016	−5.00	0.000*	−0.080 kg CO2/m2 per 1 unit NDVI increase	High attenuator
LST	0.0015	0.0003	5.00	0.000*	0.0015 kg CO2/m2 per 1°C increase	High
Night Lights	0.0004	0.0001	4.00	0.000*	0.0004 per unit light intensity	Moderate
Building Density	0.020	0.004	5.00	0.000*	0.020 kg CO2/m2 per 1% density increase	High
Traffic Density	0.025	0.005	5.00	0.000*	0.025 kg CO2/m2 per 100 vehicles/hour	High
Energy Consumption	0.028	0.004	7.00	0.000*	0.028 kg CO2/m2 per 100 kWh/m2	Highest driver
Pop Density	0.0001	0.0009	1.11	0.2678	0.0001 per 1000 inhab./km2	Not significant

* Statistically significant at $p < 0.05$. $R^2 = 0.80$, F-stat = 105.70, Prob(F) = 0.0000.

In Erbil, energy consumption is the primary emission driver (coefficient = 0.028, $t = 7.00$, $p < 0.001$), reflecting rising energy demand in residential buildings, hotels, hospitals and schools driven by population and economic growth as they combat high ambient temperatures. The average urban heat island intensity in Erbil is roughly twice that of Baghdad (0.0015 vs. 0.0008), suggesting warmer building materials and greater reliance on artificial cooling. Traffic intensity has a smaller effect (0.025) than in Baghdad, reflecting Erbil's wider, newer road network. As in Baghdad, NDVI is a crucial mitigating factor (−0.080, $p < 0.001$), and nighttime light intensity is slightly higher than Baghdad's (0.0004 vs. 0.0003), consistent with the city's expanding nighttime economic activity. Population density again fails to reach statistical significance.

5.4 Comparative Analysis and Policy Implications

Both urban settings share common emission drivers. A prominent shared characteristic is the significant negative relationship between NDVI and CO_2 emission intensity in both regions (Baghdad: −0.095, Erbil: −0.080), confirming that urban greenery supports a climate-resilient, smart-city strategy. Building density and energy consumption raise emissions in both contexts, and traffic density increases CO_2 emissions in both cities.

In terms of key differences, traffic density (0.040) is the strongest driver of emissions in Baghdad, reflecting congestion from narrower roads, older traffic infrastructure and heavier vehicle dependence. Energy consumption is the leading driver in Erbil (0.028), a result of rapid growth and new buildings and compounds requiring substantial energy for air conditioning and heating amid insufficient application of energy-efficiency standards. LST is nearly double in Erbil (0.0015) compared with Baghdad (0.0008), pointing to a need for dedicated urban heat island strategies, such as brighter, more reflective building materials.

All three hypotheses were confirmed. Investment in sustainable transportation solutions is advised for Baghdad, while Erbil should prioritize building energy efficiency and heat island mitigation. Both cities need to expand urban green cover, adopt reflective building materials, and implement smart energy grids.

5.5 Limitations

Several limitations apply to this study. VIIRS nighttime light data, used as a spatial proxy, have a coarser resolution (500–750 m) than the 250 m analysis grid, which may smooth the resulting spatial distribution of emission estimates. More significant is the lack of ground-truth emission data across both locations: the network of air quality monitoring stations is limited to five stations (two in Baghdad, three in Erbil). As a result, generic, widely published emission factors (EPA, IEA and IPCC standards) were used rather than locally validated factors, which may explain the observed 5.2% bias in the emission results. Available VHR imagery (WorldView/Pléiades) from commercial satellite sources also provided only sporadic temporal coverage over 2020–2024. Reducing these uncertainties in future work would benefit from locally measured emission inventories, denser air quality monitoring networks, Sentinel-5P atmospheric CO2 observations, and deep learning models.

6. CONCLUSION

This study has shown that combining remote sensing data (VHR) with socioeconomic factors in data-scarce arid urban regions holds considerable potential for small-scale carbon footprint mapping and modeling. By combining a bottom-up emission inventory approach with a top-down approach that redistributes spatially uniform emission estimates to higher-resolution scales via machine learning, high-resolution emission maps (kg CO_2/m^2) were produced for Baghdad's Zayouna/Mansour neighborhood and Erbil Municipal Center at the grid-cell level for 2020–2024. The proposed model achieved a high R^2 of 0.78 and an RMSE of 0.008 kg CO_2/m^2. Distinctive emission hotspots were identified, mostly localized near major traffic arteries and business centers.

The panel data analysis revealed two distinct relationships depending on the region: traffic intensity is the most important driving force in Baghdad ($R^2 = 0.85$), while energy consumption dominates in Erbil ($R^2 = 0.80$), reflecting different urban development trajectories. Green cover (NDVI) acts as a significant emission mitigator in both cities, underscoring its role in any climate-resilient and sustainable urban planning agenda.

These findings support specific, empirically based policy guidance for urban planners. In Baghdad, priority should be given to sustainable transport solutions and traffic management. In Erbil, improvements should focus on building energy efficiency and mitigating the urban heat island effect. Both cities should expand urban green space, adopt reflective building materials, and pursue efficient energy management. The methodology presented is transferable to other data-deficient cities seeking to conduct effective, smart-city-oriented urban planning. Further research should incorporate multi-source environmental data, such as Sentinel-5P or additional climate datasets, together with deep learning approaches, to further improve classification accuracy and predictive power.

STATEMENTS AND DECLARATIONS

Funding: The author received no specific funding for this research.

Competing Interests: The author declares no competing financial or personal interests.

Ethical Compliance: No studies involving humans or animals were conducted.

Author Contributions: Conceptualization, methodology, formal analysis, visualization, and writing: Y.A.N. Aldabbagh.

Data Availability: The datasets generated and analyzed during this study are available from the corresponding author upon reasonable request.

REFERENCES

[1] Akrofi, M. M. (2025). Green hotspots? Unveiling global hotspots and shifting trends in carbon credit projects. *Sustainable Development*, 33(2), 1782–1796.

[2] Abdullah, H., Hama Sharef, S. H., Omar, D. K., & Çullu, M. A. (2024). Comparing urban heat islands in Erbil City-Iraq: Investigating vegetation response through day and night thermal analysis. *Applied Ecology and Environmental Research*, 22(2), 1917–1930.

[3] Al-Fehdly, W., ElMaraghy, W., & Wilkinson, S. (2019). Carbon footprint estimation for oil production: Iraq case study for the utilization of waste gas in generating electricity. *Procedia CIRP*, 80, 389–392.

[4] Chen, K., et al. (2022). Recent advances in carbon footprint studies of urban ecosystems: Overview, application, and future challenges. *Environmental Reviews*, 30(2), 342–356.

[5] Fang, Z., & Liu, Z. (2025). Digital innovations driving urban sustainability: Key factors in reducing carbon emissions. *Sustainability*, 17(5), 2186.

[6] Gurney, K. R., et al. (2009). High resolution fossil fuel combustion CO2 emission fluxes for the United States. *Environmental Science & Technology*, 43(14), 5535–5541.

[7] Hong, S., Fu, T., & Dai, M. (2025). Machine learning-based carbon emission predictions and customized reduction strategies for 30 Chinese provinces. *Sustainability*, 17(5), 1786.

[8] Hashim, B. M., Al Maliki, A., Sultan, M. A., et al. (2022). Effect of land use land cover changes on land surface temperature during 1984–2020: A case study of Baghdad city using Landsat image. *Natural Hazards*, 112, 1723–1746.

[9] Hu, Y., Xu, J., & Liu, T. (2025). The impact of digitalization on carbon emission efficiency. *Sustainability*, 17(14), 6551.

[10] IEA. (2023). *Iraq Energy Outlook*. International Energy Agency, Paris.

[11] IIETA. (2023). Land use/land cover changes in the Euphrates Basin (1985–2022). *International Journal of Heat and Technology*.

[12] IPCC. (2006). *2006 IPCC Guidelines for National Greenhouse Gas Inventories*. Institute for Global Environmental Strategies, Hayama, Japan.

[13] IPCC. (2022). *Climate Change 2022: Mitigation of Climate Change. Contribution of Working Group III to the Sixth Assessment Report*. Cambridge University Press.

[14] Jabbar, M. T., & Zhou, J. X. (2013). Environmental degradation assessment in arid areas: A case study from Basra Province, southern Iraq. *Environmental Earth Sciences*, 70(5), 2203–2214.

[15] Kennedy, C., et al. (2009). Greenhouse gas emissions from global cities. *Environmental Science & Technology*, 43(19), 7297–7302.

[16] Lodhi, M. K., et al. (2025). Advancing urban solar assessment: A deep learning and atmospheric modelling framework. *Energy and Buildings*, 338, 115717.

[17] Lombardi, M., et al. (2017). Assessing the urban carbon footprint: An overview. *Environmental Impact Assessment Review*, 66, 43–52.

[18] Mao, H., et al. (2025). Intellectual property rights, renewable energy innovation, and carbon emission reduction. *Energy Strategy Reviews*, 59, 101705.

[19] Mennis, J. (2003). Generating surface models of population using dasymetric mapping. *The Professional Geographer*, 55(1), 31–42.

[20] Mirabella, N., & Allacker, K. (2018). The assessment of urban environmental impacts through the city environmental footprint. *Procedia CIRP*, 69, 83–88.

[21] Moran, D., et al. (2018). Carbon footprints of 13,000 cities. *Environmental Research Letters*, 13(6), 064041.

[22] Muñoz-Arango, A. M., et al. (2025). Methodology for estimating indirect emissions from Scope 3. *Journal of Cleaner Production*, 495, 145017.

[23] Onojeghuo, A., Rasul, A., & Onojeghuo, A. (2025). Air pollution exposure and hotspots of CO, NO2, SO2, PM2.5, and aerosols in Iraq. *Environmental Monitoring and Assessment*, 197(11), 1226.

[24] Pérez, J., et al. (2018). Evaluating carbon footprint of municipal solid waste treatment. *Journal of Cleaner Production*, 205, 419–431.

[25] Singh. R., Verghese. S. P., Bansal A. (2026). Silver Nanoparticles For Environmental Sustainability And Their Role In Biological Activities. International Journal of Engineering Sciences & Research Technology, 15(3), 1–8. ttps://doi.org/10.64149/j.ijesrt.15.3-1-8

[26] Piao, L., et al. (2025). Carbon emission from land use in Yanshan-Taihang Mountain area. *Applied Sciences*, 15(4), 1886.

[27] Rasul, A., Balzter, H., & Smith, C. (2016). Diurnal and seasonal variation of surface urban cool and heat islands in the semi-arid city of Erbil, Iraq. *Climate*, 4(3), 42.

[28] Sadri-Shojaei, S., Momeni, M., & Kerachian, R. (2025). A novel methodology for assessing resources and environmental carrying capacity. *Journal of Environmental Management*, 373, 123507.

[29] Tang, D., Yao, Y., & Li, X. (2025). Global consumption-based deforestation carbon emissions and regional hotspots. *Earth System Science Data Discussions*, 1–20.

[30] Tissologo M., Seydou Ouedraogo S., Nikiema O., Salami A. A.,(2026). Analysis of the Impact of Integrating A Hybrid Pv/Lng Power Plant into The National Interconnected Grid of Burkina Faso. International Journal of Engineering Sciences & Research Technology, 15(5), 116-121 https://doi.org/10.64149/j.ijesrt.15.5.116-121

[31] United Nations. (2018). *World Urbanization Prospects: The 2018 Revision*. Department of Economic and Social Affairs, Population Division.

[32] US EPA. (2021). *Emission Factors for Greenhouse Gas Inventories*. United States Environmental Protection Agency.

[33] Ye, X., et al. (2025). Data-driven neighborhood-level carbon emission accounting models and decarbonization strategies. *Sustainable Cities and Society*, 125, 106346.